

Direct Multipath-Based SLAM: Supporting Document

Mingchao Liang, Erik Leitinger, and Florian Meyer

This manuscript provides derivations and further experimental results for the publication, “Direct Multipath-Based SLAM” by the same authors [1].

1 Computation of Matrices $\mathbf{C}_{\iota,k}^{(j)}(\mathbf{x}_k)$, $\mathbf{C}_{\kappa,k,n}^{(j)}(\phi_{k,n}^{(j)})$, and $\mathbf{C}_{\nu,k}^{(j)}$

In this section, we present the derivation of the covariance matrices in [1, (28)-(30)]. By definition, $\mathbf{C}_{\kappa,k,n}^{(j)}$ is computed as

$$\begin{aligned} \mathbf{C}_{\kappa,k,n}^{(j)}(\phi_{k,n}^{(j)}) &= \int \mathbf{z}_k^{(j)} \mathbf{z}_k^{(j)H} \kappa(\mathbf{y}_{k,n}^{(j)}; \mathbf{z}_k^{(j)}) d\mathbf{z}_k^{(j)} \\ &= \sum_{r_{k,1}^{(j)} \in \{0,1\}} \cdots \sum_{r_{k,n-1}^{(j)} \in \{0,1\}} \sum_{r_{k,n+1}^{(j)} \in \{0,1\}} \cdots \sum_{r_{k,N_k}^{(j)} \in \{0,1\}} \int \cdots \int \left(\int \mathbf{z}_k^{(j)} \mathbf{z}_k^{(j)H} f(\mathbf{z}_k^{(j)} | \mathbf{x}_k, \mathbf{y}_k^{(j)}, \eta_k^{(j)}) d\mathbf{z}_k^{(j)} \right) \\ &\quad \times \xi(\eta_k^{(j)}) \beta(\mathbf{x}_k) \prod_{\substack{n'=1 \\ n' \neq n}}^{N_k^{(j)}} \alpha(\mathbf{y}_{k,n'}^{(j)}) d\phi_{k,1}^{(j)} \cdots d\phi_{k,n-1}^{(j)} d\phi_{k,n+1}^{(j)} \cdots d\phi_{k,N_k}^{(j)} d\eta_k^{(j)} d\mathbf{x}_k \end{aligned} \quad (1)$$

where $\int \mathbf{z}_k^{(j)} \mathbf{z}_k^{(j)H} f(\mathbf{z}_k^{(j)} | \mathbf{x}_k, \mathbf{y}_k^{(j)}, \eta_k^{(j)}) d\mathbf{z}_k^{(j)} = \mathbf{C}_{k,n}^{(j)} = \eta_k^{(j)} \mathbf{I}_M + \sum_{n=1}^{N_k^{(j)}} r_{k,n}^{(j)} \gamma_{k,n}^{(j)} \mathbf{h}_{k,n}^{(j)} \mathbf{h}_{k,n}^{(j)H}$ as discussed in [1, Sec. II-B]. Plugging in the result we obtain

$$\begin{aligned} \mathbf{C}_{\kappa,k,n}^{(j)}(\phi_{k,n}^{(j)}) &= \sum_{r_{k,1}^{(j)} \in \{0,1\}} \cdots \sum_{r_{k,n-1}^{(j)} \in \{0,1\}} \sum_{r_{k,n+1}^{(j)} \in \{0,1\}} \cdots \sum_{r_{k,N_k}^{(j)} \in \{0,1\}} \int \cdots \int \left(\eta_k^{(j)} \mathbf{I}_M + \sum_{n=1}^{N_k^{(j)}} r_{k,n}^{(j)} \gamma_{k,n}^{(j)} \mathbf{h}_{k,n}^{(j)} \mathbf{h}_{k,n}^{(j)H} \right) \\ &\quad \times \xi(\eta_k^{(j)}) \beta(\mathbf{x}_k) \prod_{\substack{n'=1 \\ n' \neq n}}^{N_k^{(j)}} \alpha(\mathbf{y}_{k,n'}^{(j)}) d\phi_{k,1}^{(j)} \cdots d\phi_{k,n-1}^{(j)} d\phi_{k,n+1}^{(j)} \cdots d\phi_{k,N_k}^{(j)} d\eta_k^{(j)} d\mathbf{x}_k \\ &= \sum_{r_{k,1}^{(j)} \in \{0,1\}} \cdots \sum_{r_{k,n-1}^{(j)} \in \{0,1\}} \sum_{r_{k,n+1}^{(j)} \in \{0,1\}} \cdots \sum_{r_{k,N_k}^{(j)} \in \{0,1\}} \int \cdots \int \left(\sum_{n=1}^{N_k^{(j)}} r_{k,n}^{(j)} \gamma_{k,n}^{(j)} \mathbf{h}_{k,n}^{(j)} \mathbf{h}_{k,n}^{(j)H} \right) \\ &\quad \times \beta(\mathbf{x}_k) \prod_{\substack{n'=1 \\ n' \neq n}}^{N_k^{(j)}} \alpha(\mathbf{y}_{k,n'}^{(j)}) d\phi_{k,1}^{(j)} \cdots d\phi_{k,n-1}^{(j)} d\phi_{k,n+1}^{(j)} \cdots d\phi_{k,N_k}^{(j)} + \int \eta_k^{(j)} \mathbf{I}_M \xi(\eta_k^{(j)}) d\eta_k^{(j)} \end{aligned}$$

$$\begin{aligned}
&= r_{k,n}^{(j)} \gamma_{k,n}^{(j)} \int \mathbf{h}_{k,n}^{(j)} \mathbf{h}_{k,n}^{(j)H} \beta(\mathbf{x}_k) d\mathbf{x}_k + \sum_{\substack{n'=1 \\ n' \neq n}}^{N_k^{(j)}} r_{k,n'}^{(j)} \sum_{\mathbf{y}_{k,n'}^{(j)} \in \{0,1\}} \int r_{k,n'}^{(j)} \gamma_{k,n'}^{(j)} \mathbf{h}_{k,n'}^{(j)} \mathbf{h}_{k,n'}^{(j)H} \alpha(\mathbf{y}_{k,n'}^{(j)}) \beta(\mathbf{x}_k) d\phi_{k,n'}^{(j)} d\mathbf{x}_k \\
&\quad + \int \eta_k^{(j)} \mathbf{I}_M \xi(\eta_k^{(j)}) d\eta_k^{(j)} \\
&= r_{k,n}^{(j)} \gamma_{k,n}^{(j)} \int \mathbf{h}_{k,n}^{(j)} \mathbf{h}_{k,n}^{(j)H} \beta(\mathbf{x}_k) d\mathbf{x}_k + \sum_{\substack{n'=1 \\ n' \neq n}}^{N_k^{(j)}} \int \gamma_{k,n'}^{(j)} \mathbf{h}_{k,n'}^{(j)} \mathbf{h}_{k,n'}^{(j)H} \alpha(\phi_{k,n'}^{(j)}, 1) \beta(\mathbf{x}_k) d\phi_{k,n'}^{(j)} d\mathbf{x}_k \\
&\quad + \int \eta_k^{(j)} \mathbf{I}_M \xi(\eta_k^{(j)}) d\eta_k^{(j)} \\
&= r_{k,n}^{(j)} \mathbf{C}_{2,k,n}^{(j)}(\phi_{k,n}^{(j)}) + \sum_{\substack{n'=1 \\ n' \neq n}}^{N_k^{(j)}} \mathbf{C}_{3,k,n'}^{(j)} + \eta_{\xi,k}^{(j)} \mathbf{I}_M.
\end{aligned} \tag{2}$$

which is the same as [1, (28)-(30)]. The matrices $\mathbf{C}_{l,k}^{(j)}(\mathbf{x}_k)$ and $\mathbf{C}_{\nu,k}^{(j)}$ can be derived in a similar way.

2 Monte Carlo Integration of $\mathbf{C}_{1,k,n}^{(j)}(\mathbf{x}_k)$, $\mathbf{C}_{2,k,n}^{(j)}(\phi_{k,n}^{(j)})$, and $\mathbf{C}_{3,k,n}^{(j)}$

In this section, we discuss how the “stacking technique” from [1, (39)-(41)] is used within our direct SLAM framework. We start from the “non-stacked” Monte Carlo integration of $\mathbf{C}_{3,k,n}^{(j)}$

$$\mathbf{C}_{3,k,n}^{(j)} \approx \sum_{p=1}^P \sum_{p'=1}^P w_{\beta,k}^{(p)} w_{\alpha,k,n}^{(j,p')} \mathbf{H}_{k,n}(\mathbf{x}_k^{(p)}, \phi_{k,n}^{(j,p')}). \tag{3}$$

This “non-stacked” version has complexity $\mathcal{O}(P^2)$. To avoid the square complexity, we stack the particles and only evaluate pairs $(p, p'), p = p'$. As a result,

$$\begin{aligned}
\mathbf{C}_{3,k,n}^{(j)} &\approx \sum_{p=1}^P w_{\beta,k}^{(p)} \left(\sum_{p'=1}^P w_{\alpha,k,n}^{(j,p')} \right) \mathbf{H}_{k,n}(\mathbf{x}_k^{(p)}, \phi_{k,n}^{(j,p)}) \\
&= \sum_{p=1}^P w_{\beta,k}^{(p)} \left(\sum_{p'=1}^P w_{\alpha,k,n}^{(j,p')} \right) \tilde{\mathbf{H}}_{k,n}^{(j,p)} = \tilde{\mathbf{C}}_{3,k,n}^{(j)}.
\end{aligned} \tag{4}$$

Similarly, $\mathbf{C}_{1,k,n}^{(j)}(\mathbf{x}_k)$ and $\mathbf{C}_{2,k,n}^{(j)}(\phi_{k,n}^{(j)})$ are approximated as

$$\begin{aligned}
\mathbf{C}_{1,k,n}^{(j)}(\mathbf{x}_k^{(p)}) &\approx \sum_{p'=1}^P w_{\alpha,k,n}^{(j,p')} \mathbf{H}_{k,n}(\mathbf{x}_k^{(p)}, \phi_{k,n}^{(j,p')}) \\
&\approx \left(\sum_{p'=1}^P w_{\alpha,k,n}^{(j,p')} \right) \mathbf{H}_{k,n}(\mathbf{x}_k^{(p)}, \phi_{k,n}^{(j,p)}) \\
&= \left(\sum_{p'=1}^P w_{\alpha,k,n}^{(j,p')} \right) \tilde{\mathbf{H}}_{k,n}^{(j,p)} = \tilde{\mathbf{C}}_{1,k,n}^{(j)}(\mathbf{x}_k^{(p)})
\end{aligned} \tag{5}$$

$$\mathbf{C}_{2,k,n}^{(j)}(\phi_{k,n}^{(j,p)}) \approx \sum_{p'=1}^P w_{\beta,k}^{(p')} \mathbf{H}_{k,n}(\mathbf{x}_k^{(p')}, \phi_{k,n}^{(j,p)})$$

$$\begin{aligned}
&\approx \left(\sum_{p'=1}^P w_{\beta,k}^{(j,p')} \right) \mathbf{H}_{k,n}(\mathbf{x}_k^{(p)}, \phi_{k,n}^{(j,p)}) \\
&= \mathbf{H}_{k,n}(\mathbf{x}_k^{(p)}, \phi_{k,n}^{(j,p)}) = \tilde{\mathbf{H}}_{k,n}^{(j,p)} = \tilde{\mathbf{C}}_{2,k,n}^{(j)}(\phi_{k,n}^{(j,p)}).
\end{aligned} \tag{6}$$

3 Alternative Approximation of Measurement Update Messages

As discussed in [1, Sec. III-C], the measurement update messages $\iota(\mathbf{x}_k; \mathbf{z}_k^{(j)})$, $\kappa(\mathbf{y}_{k,n}^{(j)}; \mathbf{z}_k^{(j)})$, and $\nu(\eta_k^{(j)}; \mathbf{z}_k^{(j)})$ are approximated by Gaussian density functions with respect to $\mathbf{z}_k^{(j)}$, and the covariance matrices of the Gaussian probability density functions (PDFs) are computed using moment matching. Since evaluating Gaussian PDFs requires the inverse of the covariance matrices, the computational complexity scales cubically with the number of measurements M . In this section, we provide an alternative approximation that reduces the complexity.

The main idea used for the derivation of alternative measurement update messages is to use the outer product of the mean vector to approximate the correlation (covariance) matrix. Specifically, we now compute an alternative approximation of [1, (33)] based on the outer product $\mathbf{C}_{3,k,n}^{(j)} = \boldsymbol{\mu}_{3,k,n}^{(j)} \boldsymbol{\mu}_{3,k,n}^{(j)\text{H}}$, where

$$\boldsymbol{\mu}_{3,k,n}^{(j)} = \int \sqrt{\gamma_{k,n}^{(j)}} \mathbf{h}_{k,n}^{(j)} \alpha(\phi_{k,n}^{(j)}, 1) \beta(\mathbf{x}_k) d\phi_{k,n}^{(j)} d\mathbf{x}_k.$$

A particle-based computation of this outer product [1, (41)] is then computed as $\tilde{\mathbf{C}}_{3,k,n}^{(j)} = \tilde{\boldsymbol{\mu}}_{3,k,n}^{(j)} \tilde{\boldsymbol{\mu}}_{3,k,n}^{(j)\text{H}}$ with

$$\tilde{\boldsymbol{\mu}}_{3,k,n}^{(j)} = \sum_{p=1}^P w_{\beta,k}^{(p)} \left(\sum_{p'=1}^P w_{\alpha,k,n}^{(j,p')} \right) \sqrt{\gamma_{k,n}^{(j,p)}} \mathbf{h}_{k,n}^{(j,p)}.$$

Based on this approximation, the matrix $\tilde{\mathbf{C}}_{\kappa,k,n}^{(j)}(\mathbf{y}_{k,n}^{(j,p)})$ now reads

$$\begin{aligned}
\tilde{\mathbf{C}}_{\kappa,k,n}^{(j)}(\mathbf{y}_{k,n}^{(j,p)}) &= r_{k,n}^{(j)} \gamma_{k,n}^{(j,p)} \mathbf{h}_{k,n}^{(j,p)} \mathbf{h}_{k,n}^{(j,p)\text{H}} + \sum_{\substack{n'=1 \\ n' \neq n}}^{N_k^{(j)}} \tilde{\boldsymbol{\mu}}_{3,k,n'}^{(j)} \tilde{\boldsymbol{\mu}}_{3,k,n'}^{(j)\text{H}} + \tilde{\eta}_{\xi,k}^{(j)} \mathbf{I}_M \\
&= r_{k,n}^{(j)} \gamma_{k,n}^{(j,p)} \mathbf{h}_{k,n}^{(j,p)} \mathbf{h}_{k,n}^{(j,p)\text{H}} + \mathbf{B}_{k,n}^{(j)} \mathbf{B}_{k,n}^{(j)\text{H}} + \tilde{\eta}_{\xi,k}^{(j)} \mathbf{I}_M \\
&= r_{k,n}^{(j)} \gamma_{k,n}^{(j,p)} \mathbf{h}_{k,n}^{(j,p)} \mathbf{h}_{k,n}^{(j,p)\text{H}} + \mathbf{A}_{k,n}^{(j)}
\end{aligned} \tag{7}$$

with $\mathbf{B}_{k,n}^{(j)} = [\tilde{\boldsymbol{\mu}}_{3,k,1}^{(j)} \cdots \tilde{\boldsymbol{\mu}}_{3,k,n-1}^{(j)} \tilde{\boldsymbol{\mu}}_{3,k,n+1}^{(j)} \cdots \tilde{\boldsymbol{\mu}}_{3,k,N_k^{(j)}}^{(j)}] \in \mathbb{C}^{M \times (N_k^{(j)}-1)}$ and $\mathbf{A}_{k,n}^{(j)} = \mathbf{B}_{k,n}^{(j)} \mathbf{B}_{k,n}^{(j)\text{H}} + \tilde{\eta}_{\xi,k}^{(j)} \mathbf{I}_M$. To evaluate $\mathcal{CN}(\mathbf{z}_k^{(j)}; \mathbf{0}, \tilde{\mathbf{C}}_{\kappa,k,n}^{(j)}(\mathbf{y}_{k,n}^{(j,p)}))$ for $\tilde{w}_{\mathbf{y},k,n}^{(j,p)}$ [1, (44)], one needs to compute the quantities $\det(\tilde{\mathbf{C}}_{\kappa,k,n}^{(j)}(\mathbf{y}_{k,n}^{(j,p)}))$ and $\mathbf{z}_k^{(j)\text{H}} (\tilde{\mathbf{C}}_{\kappa,k,n}^{(j)}(\mathbf{y}_{k,n}^{(j,p)}))^{-1} \mathbf{z}_k^{(j)}$, which can be computed efficiently using the matrix determinant lemma and matrix inversion lemma, respectively, as

$$\begin{aligned}
\det(\tilde{\mathbf{C}}_{\kappa,k,n}^{(j)}(\mathbf{y}_{k,n}^{(j,p)})) &= \det(r_{k,n}^{(j)} \gamma_{k,n}^{(j,p)} \mathbf{h}_{k,n}^{(j,p)} \mathbf{h}_{k,n}^{(j,p)\text{H}} + \mathbf{A}_{k,n}^{(j)}) \\
&= \det(1 + r_{k,n}^{(j)} \gamma_{k,n}^{(j,p)} \mathbf{h}_{k,n}^{(j,p)\text{H}} (\mathbf{A}_{k,n}^{(j)})^{-1} \mathbf{h}_{k,n}^{(j,p)}) \det(\mathbf{A}_{k,n}^{(j)})
\end{aligned} \tag{8}$$

$$\begin{aligned}
\mathbf{z}_k^{(j)\text{H}} (\tilde{\mathbf{C}}_{\kappa,k,n}^{(j)}(\mathbf{y}_{k,n}^{(j,p)}))^{-1} \mathbf{z}_k^{(j)} &= \mathbf{z}_k^{(j)\text{H}} (r_{k,n}^{(j)} \gamma_{k,n}^{(j,p)} \mathbf{h}_{k,n}^{(j,p)} \mathbf{h}_{k,n}^{(j,p)\text{H}} + \mathbf{A}_{k,n}^{(j)})^{-1} \mathbf{z}_k^{(j)} \\
&= \mathbf{z}_k^{(j)\text{H}} (\mathbf{A}_{k,n}^{(j)})^{-1} \mathbf{z}_k^{(j)} - \frac{r_{k,n}^{(j)} \gamma_{k,n}^{(j,p)} |\mathbf{h}_{k,n}^{(j,p)\text{H}} (\mathbf{A}_{k,n}^{(j)})^{-1} \mathbf{z}_k^{(j)}|^2}{1 + r_{k,n}^{(j)} \gamma_{k,n}^{(j,p)} \mathbf{h}_{k,n}^{(j,p)\text{H}} (\mathbf{A}_{k,n}^{(j)})^{-1} \mathbf{h}_{k,n}^{(j,p)}}.
\end{aligned} \tag{9}$$

Table 1: Average runtime of different methods per time step

Method	Time (s)		
	300MHz	400MHz	600MHz
Direct-SLAM	1.19	1.53	2.58
Direct-SLAM-fast	0.74	0.88	1.25

Next, $(\mathbf{A}_{k,n}^{(j)})^{-1}$ can be further factorized again using the matrix inversion lemma

$$\begin{aligned}
(\mathbf{A}_{k,n}^{(j)})^{-1} &= \left(\mathbf{B}_{k,n}^{(j)} \mathbf{B}_{k,n}^{(j)\text{H}} + \tilde{\eta}_{\xi,k}^{(j)} \mathbf{I}_M \right)^{-1} \\
&= \left(\tilde{\eta}_{\xi,k}^{(j)} \right)^{-1} \mathbf{I}_M - \left(\tilde{\eta}_{\xi,k}^{(j)} \right)^{-1} \mathbf{B}_{k,n}^{(j)} \left(\mathbf{B}_{k,n}^{(j)\text{H}} \mathbf{B}_{k,n}^{(j)} + \tilde{\eta}_{\xi,k}^{(j)} \mathbf{I}_{N_k^{(j)}-1} \right)^{-1} \mathbf{B}_{k,n}^{(j)\text{H}}
\end{aligned} \tag{10}$$

with which the quantities $\mathbf{z}_k^{(j)\text{H}} (\mathbf{A}_{k,n}^{(j)})^{-1} \mathbf{z}_k^{(j)}$, $\mathbf{h}_{k,n}^{(j,p)\text{H}} (\mathbf{A}_{k,n}^{(j)})^{-1} \mathbf{z}_k^{(j)}$, and $\mathbf{h}_{k,n}^{(j,p)\text{H}} (\mathbf{A}_{k,n}^{(j)})^{-1} \mathbf{h}_{k,n}^{(j,p)}$ can be computed in $\mathcal{O}(N_k^{(j)} M + (N_k^{(j)})^3)$ instead of in $\mathcal{O}(M^3)$. Note that since $\det(\mathbf{A}_{k,n}^{(j)})$ appears in both the numerator and denominator of $\tilde{w}_{y,k,n}^{(j,p)}$ [1, (44)] and does thus not need to be computed. The same method can be applied to the computation of $\tilde{w}_{x,k}^{(p)}$ and $\tilde{w}_{\eta,k}^{(j,p')}$ [1, (43), (45)]. Including the operations of all particles and potential features (PFs), as well as the initialization of new PFs, the total complexity is $\mathcal{O}\left(M^2 + P\left(\sum_{j=1}^J (N_k^{(j)})^2 M + \sum_{j=1}^J (N_k^{(j)})^4\right)\right)$ which scales quadratically with the number of measurements M . The number of PFs $N_k^{(j)}$ is typically smaller than ten and having five features is already sufficient to accurately localize the agent. Hence, this alternative approximation has time complexity advantages over the original one in high-bandwidth cases.

Next we repeat the experiments in [1, Sec. V-B] to show the efficacy of the alternative approximation that we refer to as “Direct-SLAM-fast”. All the parameter settings remain the same. The results are shown in Figure 1, from which we can see that Direct-SLAM-fast has almost identical performance compared with the original Direct-SLAM. The averaged runtime shown in Table 1 verifies that Direct-SLAM-fast achieves lower computational complexity in the considered bandwidths.

4 Qualitative Real Data Results

The real radio measurements have been collected in a room with the floorplan as shown in [1, Fig. 4], and the two physical anchors (PAs) are in the same positions as well. The mobile agent moves following a track composed of 679 consecutive positions shown as yellow line in [1, Fig. 4], yet the accurate position of the agent at each time step is not available. The radio signals are measured with a vector network analyzer (VNA) over a bandwidth of $B = 2$ GHz at a center frequency of $f_c = 3$ GHz. The dipole-like ultra-wideband transmit antenna mounted at the mobile agent and the dipole-like ultra-wideband receiver antennas mounted at two static PAs have a uniform radiation pattern in the azimuth plane and nulls in the ground and ceiling directions. Using $S(f)$, the measured radio signals are filtered to a bandwidth of $B = 400$ MHz and demodulated to received baseband signals $\mathbf{z}_k^{(j)}$, $j \in \{1, 2\}$ with $M = 41$. The magnitude spectrum $|\tilde{z}_{k,m}^{(j)}|$, $j \in \{1, 2\}$ of the real measurements used by the Direct-SLAM algorithm is shown in Figure 2a-2b. Compared to simulated radio signals shown in [1, Fig. 5], it can be observed that the real measurements contain more measurement noise and non-specular multipath effects, including dense multipath component (DMC).

For the experiments running on real data, we set the driving noise variance for legacy PF positions $\sigma_{\mathbf{p},n}^2$ to $2.5 \times 10^{-5} \text{ m}^2$ for PAs, and to $6.4 \times 10^{-5} \text{ m}^2$ for other virtual anchors (VAs). Increasing driving noise variance improves robustness in this scenario. All other parameters remain the same as in [1, Sec. V-A]. Since there are no ground truth agent positions, we present a qualitative result in Figure 2c. It can be seen that some

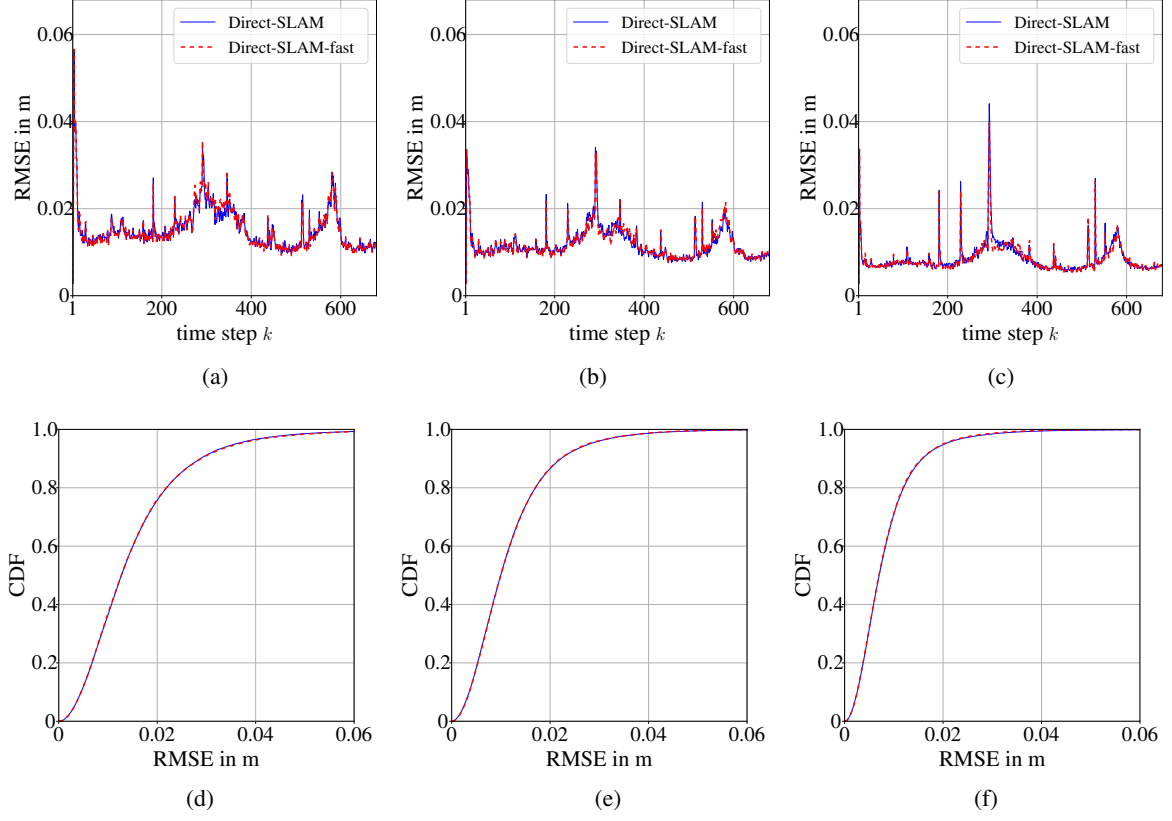


Figure 1: Performance of agent localization on synthetic data: The first row shows the agent position RMSEs averaged over 100 simulation runs with (a) 300 MHz, (b) 400 MHz, and (c) 600 MHz bandwidth, respectively. The second row shows the empirical CDFs of the RMSEs with (d) 300 MHz, (e) 400 MHz, and (f) 600 MHz bandwidth, respectively.

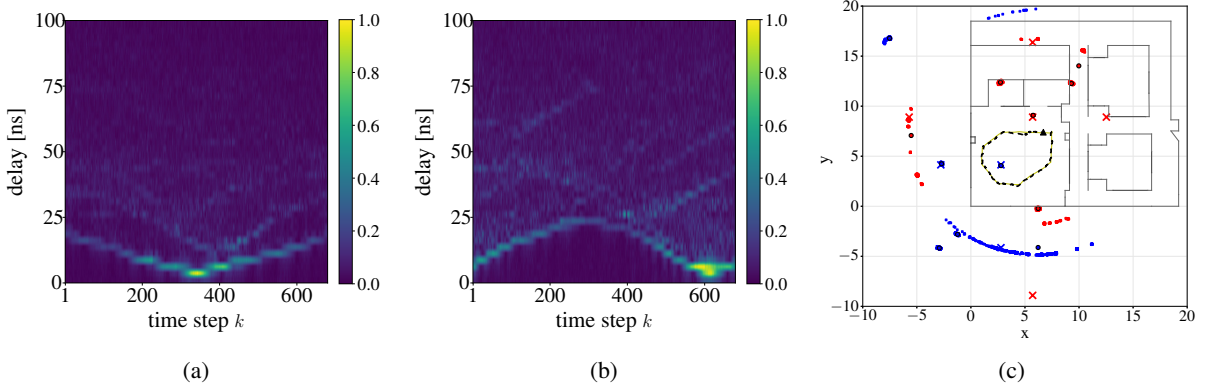


Figure 2: The magnitude spectrum $|\tilde{z}_{k,m}^{(j)}|$ of real data with 400MHz bandwidth and normalized to $[0, 1]$ of PA (a) $j = 1$ and (b) $j = 2$.

estimated PFs do not relate to any specular path. These result from the fact that real measurements include non-specular multipath components (MPCs) and there is a model mismatch. Nonetheless, the proposed Direct-SLAM algorithm is still able to provide reasonable estimates for the agent position and the features in the environment.

References

- [1] M. Liang, E. Leitingner, and F. Meyer, “Direct multipath-based SLAM,” *IEEE Trans. Signal Process.*, 2025.